

Adsorption, diffusion, and vibration of oxygen on Ag(110)Takat B. Rawal,¹ Sampyo Hong,^{1,2,*} Aki Pulkkinen,³ Matti Alatalo,⁴ and Talat S. Rahman¹¹*Department of Physics, University of Central Florida, Orlando, Florida 32816, USA*²*Department of Physics, University of North Florida, Jacksonville, Florida 32225, USA*³*Department of Mathematics and Physics, Lappeenranta University of Technology, P. O. Box 20, FI-53851, Finland*⁴*Center of molecular materials, Faculty of science, University of Oulu, P. O. Box 8000, FI-90014, Finland*

(Received 15 April 2015; published 31 July 2015)

We have employed *ab initio* density functional theory (DFT) to study the adsorption, dissociation, diffusion, and vibration of oxygen on Ag(110). We find that the fourfold-hollow site is the preferred site for O₂ adsorption and that the O₂ molecular axis marginally prefers to align along the [1 $\bar{1}$ 0] direction (for which the adsorption energy is -0.41 eV) rather than along the [001] (for which it is -0.37 eV). By weakening the O-O bond, the net charge transfer of $\sim 0.9e$ from Ag to the antibonding orbital ($2\pi^*$) of O₂ facilitates dissociation of O₂ on Ag(110). Contrary to a previous theoretical suggestion (subsequently incorporated into interpretation of an experiment), our DFT calculations for adsorption energies and dissociation energy barriers, taken together with findings concerning vibrational frequencies and charge transfer, indicate that, when adsorbing, O₂ prefers to align along the [1 $\bar{1}$ 0] direction, and when dissociating, does align along the [001] direction with the dissociated O atoms adsorbing onto threefold-hollow sites rather than short-bridge sites. Importantly, our calculations clearly show that dissociation of O₂ on Ag(110) is coupled with the surface Rayleigh mode (~ 4 meV) and O₂ dissociation along the [001] direction is more strongly coupled with the substrate motion than O₂ dissociation along the [1 $\bar{1}$ 0] direction indicating that O₂ dissociation (particularly, O₂[001]) can be activated by surface phonon even at quite low temperature. Once thus dissociated, the O atoms can more easily diffuse in the [1 $\bar{1}$ 0] direction, from one fourfold-hollow site to the next owing to a smaller diffusion barrier in the latter.

DOI: [10.1103/PhysRevB.92.035444](https://doi.org/10.1103/PhysRevB.92.035444)

PACS number(s): 31.15.A-, 68.43.Jk, 68.43.Pq

I. INTRODUCTION

Silver is an important catalyst for oxidation reactions in industry. It is used as a catalyst for the oxidative dehydrogenation of methanol [1], the photolysis of molecular oxygen (O₂) at high coverage [2], and the epoxidation of ethylene [3,4]. Accordingly, Ag surfaces have been extensively investigated over the last decades. As the most corrugated surface among the low-Miller-index surfaces of Ag, the (110) surface's interaction with gas molecules such as oxygen proceeds via such fundamental physical processes as adsorption and dissociation. For accurate manipulation of such gas-surface interactions [5–7], and of the oxidation reactions of CO [8,9] and hydrocarbons [10] on Ag(110), it is essential to understand the surface structures of various phases of oxygen moieties formed on Ag(110) upon the adsorption and dissociation of O₂. The microscopic characterization of such adsorbed species is of general interest for understanding the catalytic activity of Ag(110). Such understanding may provide insights into the mechanisms that enable enhancement of the catalytic oxidation reaction at the large scale.

Extensive and various experimental investigation of the O₂/Ag(110) system over the last few decades has led to substantial understanding of the gas-surface dynamics and oxidation reactions. Scanning tunneling microscopy (STM) studies [9,11], for example, have shown that some adsorption modes of O₂ on Ag(110) are closely connected to the activity of the surface in CO oxidation—specifically, that CO oxidation occurs at $T > 90$ K, and that dissociated O atoms act as the reaction intermediates on the surface [11].

Another earlier STM study [12] has shown that on Ag(110) O₂ molecules serve as chemisorbed, but transient, highly mobile hot precursors which can be trapped by some other stabilized adsorbates, a phenomenon of catalytic significance as it relates to complex surface reactions associated with heterogeneous catalysis. High-energy [13] and medium-energy [14] ion-scattering experiments have shown that at room temperature the spacing between the first and second layers contracts but that between the second and third layers expands, that this multilayer relaxation is oscillatory, and that the first-two layers exhibit anisotropy in vibrational amplitude. The reflection-anisotropy spectroscopy (RAS) experiment [15] has shown that transitions between occupied and unoccupied surface states near the Y point in the Brillouin zone (BZ) are responsible for resonance in reflection anisotropy from the Ag(110) surface and, in particular, that this anisotropy stems from dipole transitions among the surface states at the Y point in the BZ. An angle-resolved photoemission study [16] has shown that oxygen adsorbs on Ag(110) in three distinct modes: a molecular physisorbed (weakly bound) mode at $T < 40$ K, a molecular chemisorbed mode between 60 and 180 K, and a dissociated chemisorbed (i.e., atomic) mode at $T > 180$ K. Electron-energy-loss spectroscopy (EELS) and thermal-desorption spectroscopy (TDS) studies [17] have observed two chemisorbed species of O₂ on Ag(110): (1) α -O₂, which was oriented along the [001] direction with a vibrational frequency of 79.5 meV and formed as a result of the conversion of the physisorbed precursor at 100 K, and (2) β -O₂, which was oriented along the [1 $\bar{1}$ 0] direction with a vibrational frequency of 85 meV and formed upon O₂ dosing at higher temperature ~ 110 K. An earlier high-resolution EELS study [18] has observed a similar trend for Ag(001)—in this instance three distinct chemisorbed O₂ species, the vibrational

*Corresponding author: Sampyo.Hong@ucf.edu

signatures of two of which are quite close to those just described. In addition, it found that, though O_2 molecules are stable below 130 K, when temperature rises above 150 K atomic oxygen (O) moieties form on the substrate, followed by a substantial change in the morphology of Ag(110) [19]. A yet earlier low-energy electron diffraction (LEED) study [20] has shown that the adsorption of O leads at 300 K to the formation of ordered ($n \times 1$) adlayer chains on Ag(110). A subsequent STM study has strongly suggested that, upon adsorption of O, Ag(110) undergoes added-row reconstruction on the step edges along the [001] direction [21]. Similarly, LEED and helium-diffraction measurements together with phonon-dispersion calculations [22] and low-energy ion-scattering measurements complemented by Monte Carlo simulation of the ion trajectories [23] have clearly demonstrated that the adsorption of O on Ag(110) results in an $O(2 \times 1)$ -Ag(110) structure, which induces a missing-row reconstruction (from the complementary point of view an added-row reconstruction) along the [001] direction, as has been shown in the analogous case of $O(2 \times 1)$ -Cu(110) [24–28].

In spite of this extensive history of investigation, there still remain unresolved issues. While O_2 preferentially adsorbs in a fourfold-hollow (FFH) site (see Fig. 1) on Ag(110), where it lies flat on the surface, its orientation (the alignment of its molecular axis with respect to the Ag rows aligned along the $[1\bar{1}0]$ direction) has been controversial. For instance, an STM study [29] concluded that tunneling electrons cause the rotation of O_2 from the [001] direction to the $[1\bar{1}0]$, so that O_2 along the $[1\bar{1}0]$ is more stable than O_2 along the [001]. Nevertheless, conclusions drawn from theoretical studies are in conflict with the above picture, as well as with each other. For example, a DFT study by Gravil *et al.* [30] shows that $O_2[001]$ is more favorable than $O_2[1\bar{1}0]$ by 40 meV. Another DFT study by Olsson *et al.* [31] claims that $O_2[001]$ and $O_2[1\bar{1}0]$ have the same adsorption energy with no preference of their two orientations. In contrast, a theoretical study [32] of the energetics and dissociation of O_2 on an Ag(110) surface of an Ag_{24} cluster shows that the chemisorbed O_2 lay along the $[1\bar{1}0]$ direction. And a recent DFT study [33] also finds

that the adsorption of O_2 with the orientation along the $[1\bar{1}0]$ is slightly more stable than that of O_2 along the [001] (the chemisorption energy of $O_2[1\bar{1}0]$ and $O_2[001]$ are found to be 0.449 and 0.439 eV, respectively). Thus, the energetic preference for the orientation of adsorbed O_2 is yet to be conclusively established, probably because energy difference between the two orientations is so small (~ 40 meV).

An STM study [29] claims that negative-voltage-biasing induced dissociation of O_2 forms an O-O complex consisting of one O atom in the FFH site and another in a short-bridge (SB) site (see Fig. 1), resulting in two dissociated O atoms (one remains in the original FFH site while the other moves away along the [001] direction) separated by more than 10 \AA ($\sim 11.7 \text{ \AA}$, the average atomic separation of dissociated O atoms [34]). The former is stable, whereas the latter is highly mobile. It also claims that O in an SB site always diffuses to another SB site, either along the [001] or $[1\bar{1}0]$ direction. The plausibility of such SB-to-SB diffusion, however, will depend on the relative stability of O in an SB with respect to that of O in other sites on Ag(110). This question of relative stability, however, remains to be investigated. Moreover, theoretical investigations so far fall short of elucidating the O diffusion pathway. Lastly, no detailed study of vibrational modes of O_2 when adsorbed on Ag(110) that could induce its dissociation has yet been performed.

To address these gaps in our understanding—the orientation of an adsorbed O_2 , the source and effect of the energy that promotes dissociation of O_2 , and the nature of the diffusion path of atomic O after dissociation—we have carried out DFT calculations to systematically examine the relaxed geometrical structures, associated electronic properties, and energetics involved in the adsorption, dissociation, diffusion, and vibration of oxygen on Ag(110).

The rest of the paper is organized as follows: we describe our theoretical methods in Sec. II, discuss our DFT results in Sec. III, and present our conclusions in Sec. IV.

II. THEORETICAL METHODS

Our model system of Ag(110) is shown in Fig. 1. There are five key adsorption sites on the (110) surface—namely, fourfold-hollow (FFH), threefold-hollow (TFH), on-top (TP), short-bridge (SB), and long-bridge (LB) sites. Molecular oxygen (O_2) adsorbs with two possible orientations with its molecular axis aligned along either the $[1\bar{1}0]$ or the [001] direction.

We have performed spin-polarized density functional theory (DFT) calculations within the Kohn-Sham formalism as implemented in the Vienna *ab initio* simulation package (VASP) [35]. To describe the exchange correlation of electrons, we use the generalized-gradient approximation (GGA) in the form of the Perdew-Burke-Ernzerhof functional (PBE) [36]. We use the projector-augmented wave (PAW) [37] pseudopotential to account for ion-electron interaction. For bulk Ag we perform a series of test calculations to determine the cut-off energy and k -point grid that produce a bulk lattice constant 4.147 \AA , in good agreement with experimental value 4.086 \AA (within 1.5%) [38]. We use the kinetic energy cutoff of 500 eV for the plane-wave expansion and sample the Brillouin zone with nine irreducible k points generated according

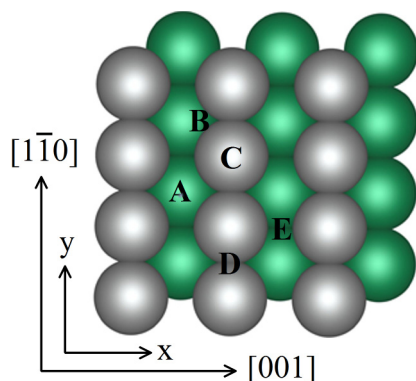


FIG. 1. (Color online) A schematic representation of Ag(110) with (3×4) surface unit cell. Light gray spheres represent Ag atoms on the top layer and light green spheres represent Ag atoms in the second layer. The possible adsorption sites for oxygen on Ag(110) are labeled as follows: A: fourfold hollow (FFH), B: threefold hollow (TFH), C: on top (TP), D: short bridge (SB), and E: long bridge (LB).

to the Monkhorst-Pack scheme [39], using the Methfessel and Paxton smearing technique [40] with a smearing width of 0.1 eV to determine the occupancy of electrons in the filled bands. To mimic Ag(110) surface, we use a (3×4) supercell of five layers with the periodic boundary condition and with 10 Å vacuum along the z direction. We use the conjugate-gradient algorithm [41,42] for the relaxation of all atoms with all degrees of freedom including the adsorbates (O_2 and its dissociated O moieties) on Ag(110). We set the criteria for the force convergence for the structural relaxation and the threshold for the total energy convergence to be 0.01 eV/Å and 10^{-4} eV, respectively.

The adsorption energy (E_{ad}) is calculated as follows: $E_{ad} = E_{(slab/adsorbate)} - (E_{(slab)} + E_{(adsorbate)})$, where $E_{(slab)}$, $E_{(adsorbate)}$, and $E_{(slab/adsorbate)}$ represent the total energies of the slab, the gas-phase adsorbates, and the slab-adsorbates complex, respectively. To determine the minimum energy pathway (MEP) with transition states for the dissociation of O_2 and diffusion of O species on Ag(110), we use the climbing-image nudged-elastic-band (CI-NEB) method [43] with five (seven in some cases) configurations (images) including the initial states and final states.

For calculation of vibrational frequencies of both atomic (O) and molecular (O_2) oxygen adsorbed on Ag(110), we use the finite-difference method as implemented in VASP. We use the dense fast Fourier transform (FFT) grids and the same high energy cutoff of 500 eV as for the ionic relaxation in order to ensure that our calculated forces are accurate, as required for reliable calculation of the vibrational frequencies. Furthermore, we take a two-step approach. In the first, we fix the substrate Ag atoms and allow the O or the O_2 species, as appropriate, to vibrate. In the second, we allow all Ag and adsorbate atoms to vibrate. We thus obtain two sets of vibrational frequencies for each oxygen species in order to detect a possible contribution of the substrate to the vibrational energy of the adsorbates. Note that a full calculation of the dispersion of the surface phonons for the oxygen-Ag(110)

system, while doable, is beyond the scope of the present work, as it would not add much to the conclusions obtained here.

We also perform Bader analysis [44,45] for estimating the charge transfer between the Ag(110) substrate and the adsorbed O or O_2 in order to see whether such changes as do occur might affect the adsorption and dissociation of O_2 , and/or diffusion of the O atom.

III. RESULTS AND DISCUSSION

A. Adsorption and dissociation of O_2 on Ag(110)

1. Adsorption of O_2

In Fig. 2 we present the calculated adsorption geometries of O_2 in the four distinct possible adsorption sites, namely FFH, SB, LB, and TP (see Fig. 1). The molecular axis of O_2 on Ag(110) lies parallel to the surface and points to one of two possible symmetrical directions: $[1\bar{1}0]$ and $[001]$. Henceforward we denote these orientations of adsorbed O_2 as $O_2[1\bar{1}0]$ and $O_2[001]$, respectively. We present the calculated structural and energetic parameters per site and orientation in Table I. Our results show that the adsorption energy of O_2 is strongly dependent on the type of adsorption site and on the axis of molecular orientation. Most importantly, we find that the most preferred adsorption site is FFH, regardless of orientation, but that for this site $O_2[1\bar{1}0]$ (-0.41 eV) is more favored than $O_2[001]$ (-0.37 eV), though by only a small margin of 40 meV. If we include the zero-point energy, the difference is further reduced to 35 meV. We note that O_2 adsorption in a long-bridge (LB) site is either weak ($E_{ad} = -0.07$ eV) or unstable, depending on the axis of orientation. At a SB site, $O_2[1\bar{1}0]$ is considerably more favorable than for $O_2[001]$, but at a LB site the opposite holds. Meanwhile, adsorption of O_2 on a TP site is unstable regardless of the axis orientation. Overall, the preferred site for O_2 adsorption on Ag(110) is FFH, as found to be similar to the case for Cu(110) [46,47] and Rh(110) [48].

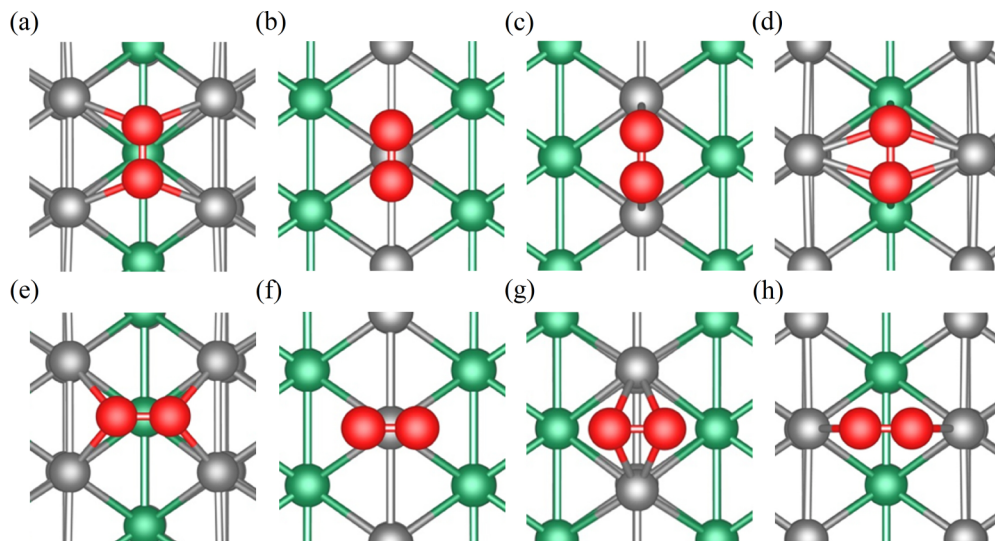


FIG. 2. (Color online) Adsorption of O_2 on Ag(110) in the following sites: (a) and (e) fourfold hollow (FFH); (b) and (f) on top (TP); (c) and (g) short bridge (SB); and (d) and (h) long bridge (LB). O_2 axis is aligned along (a)–(d) the $[1\bar{1}0]$ direction and (e)–(h) the $[001]$ direction. Color code: Ag atoms on top layer (light gray) and O atoms (red) and Ag atoms (light green) on second top layer. In the top row, the O_2 molecules are in the $[1\bar{1}0]$ orientation; in the bottom they are in the $[001]$ orientation.

TABLE I. The adsorption energy, zero-point energy, bond length, charge gained, and magnetization of O₂ on the adsorption sites at different orientations on Ag(110). $d_{\text{O-O}}$ indicates distance between the constituent O atoms; shortest $d_{\text{O-Ag}}$ indicates a distance between an O atom and the Ag closest to it.

Adsorption site	O ₂ orientation	Adsorption energy (eV)	Zero-point energy (eV)	$d_{\text{O-O}}$ (Å)	Shortest $d_{\text{O-Ag}}$ (Å)	Charge gained by O ₂ (electron)	Magnetization (μ_B)
FFH	[001]	-0.37	0.101	1.428	2.331	0.90	0.08
	[1 $\bar{1}$ 0]	-0.41	0.106	1.465	2.348	0.95	0.00
TP	[001]	0.45	-0.016	1.328	2.337	0.54	0.48
	[1 $\bar{1}$ 0]	0.42	0.072	1.329	2.372	0.55	1.41
SB	[001]	0.12	0.068	1.412	2.345	0.81	0.04
	[1 $\bar{1}$ 0]	-0.07	0.113	1.341	2.211	0.71	0.21
LB	[001]	-0.07	0.085	1.334	2.231	0.64	0.00
	[1 $\bar{1}$ 0]	0.07	0.070	1.470	2.458	0.98	0.00

The relative preferences of O₂ orientation displayed in Table I may arise from differences in the effectiveness in formation of bonds with the neighboring Ag atoms. For example, the adsorption of O₂[1 $\bar{1}$ 0] and O₂[001] at TP leads to the formation of an identical number of O-Ag bonds. In both cases, bond formation is affected by the first-nearest-neighbor interaction of the adsorbed O₂. However, if we take into account the second-nearest-neighbor interaction, then only O₂[1 $\bar{1}$ 0] leads to two additional O-Ag bonds. The energetic preference of O₂[1 $\bar{1}$ 0] is thus related to surface coordination. When O₂ adsorbs in FFH, both orientations lead to the formation of the same number of O-Ag bonds (2) by each constituent atom of O₂[1 $\bar{1}$ 0] and O₂[001] with the nearest neighboring Ag atoms in the topmost layer, so that the energetic difference between O₂[1 $\bar{1}$ 0] and O₂[001] is small (40 meV). Still, O₂[1 $\bar{1}$ 0] is energetically more favorable than O₂[001], suggesting that for O₂ in FFH, O-O repulsion in O₂[001] is stronger than that in O₂[1 $\bar{1}$ 0], owing to steric considerations. (Note the shorter O-O bond length of O₂[001] as compared to that of O₂[1 $\bar{1}$ 0]). For O₂ in gas phase, the calculated O-O internal bond length is 1.232 Å. But this O-O bond is substantially elongated upon O₂ adsorption on Ag(110). To be sure, the largest elongation (1.470 Å) occurs with O₂[1 $\bar{1}$ 0] adsorbed in an LB site, however, location at this site is unstable. But O₂[1 $\bar{1}$ 0] at FFH is stable, and shows the second-largest elongation (1.465 Å) of the O-O bond. The increase in elongation of the internal bond of the adsorbed O₂ over that of the molecule in the gas phase is a symptom of the strong interaction of O₂ with the Ag substrate, but the strongest stable interaction is with O₂[1 $\bar{1}$ 0] at FFH.

Gravil *et al.* [30] claim that the adsorption energy of O₂[001] in FFH site of Ag(110) is higher than that of O₂[1 $\bar{1}$ 0] by 40 meV. Olsson *et al.* [31] report, on the basis of their DFT calculations, that both orientations of the adsorbed O₂ have the same adsorption energy, of -0.37 eV. Nevertheless, both studies emphasize that there is no strong directional preference of the adsorbed O₂ in FFH, as suggested by the small energy difference between their two orientations. However, the STM measurements carried out by Hahn and Ho [29] revealed a ratio of the population of O₂[1 $\bar{1}$ 0] to that of O₂[001] of 1.41 at 45 K and 1.35 at 75 K. Thus, the statistical analysis of the relative population of two kinds of chemisorbed O₂ species reported by Hahn and Ho points in the direction of

our conclusion about which absorption orientation is the more favorable (and against the conclusions of both Gravil *et al.* and Olsson *et al.*). Moreover, our DFT-based conclusions are in line with the results of the MD simulations Bertolucci *et al.* [17] performed for physisorbed O₂ on Ag(110) (the precursor for the chemisorption our study investigates): “The lowest energy state was found with the molecule in the [1 $\bar{1}$ 0] direction between the rows of the first layer silver atoms. A second minimum, less strongly bound, was seen with the molecule having an azimuthal orientation parallel to the [001] and a tilt away from the surface of about 27°.” (Since they do not report the values of these minimums, it is not possible to know how large the difference was.)

In Fig. 3 we show the charge redistribution for O₂ in an FFH site and the substrate in O₂/Ag(110) systems. The O₂ molecule gains a substantial charge from the nearest-neighboring Ag atoms [Figs. 2(a) and 2(e)]. As shown in Fig. 3, 0.95e and 0.90e charges are transferred from the Ag surface to O₂[1 $\bar{1}$ 0] and O₂[001] adsorbed in FFH, respectively (see also Table I). Thus, both species of adsorbed O₂ have the oxidation number ~0.9 (characteristic of a peroxide). The donated charges go to the antibonding orbital ($2\pi^*$) of the adsorbed O₂, resulting in weaker O-O bonding, which manifests itself in the elongation of the O-O bond. This is why the O-O chemical bond in the peroxide state of O₂ is easily split into reactive O species under reaction conditions. The fact that slightly more electron is transferred to O₂[1 $\bar{1}$ 0] than to O₂[001] is the reason why O₂[1 $\bar{1}$ 0] has a longer O-O bond than O₂[001]. Note that our calculated charge transfer in the system under consideration is in qualitative agreement with those obtained from cluster-based DFT calculations [49–51] but not with the values that were extracted from infrared spectroscopy [52].

2. Dissociation of O₂

The minimum energy pathways (MEPs) for the dissociation of O₂ in FFH (the preferred adsorption site) along the [1 $\bar{1}$ 0] and [001] directions are displayed in Fig. 4. The transition state for dissociation of O₂[1 $\bar{1}$ 0] and O₂[001] occurs at 2.004 and 1.900 Å, respectively. The energy barriers for O₂[1 $\bar{1}$ 0] and O₂[001] dissociations turn out to be 0.50 and 0.42 eV, respectively. Our calculated values for these activation barriers for O₂[1 $\bar{1}$ 0] and O₂[001] dissociations are smaller than those (0.62 and 0.76 eV, respectively) calculated

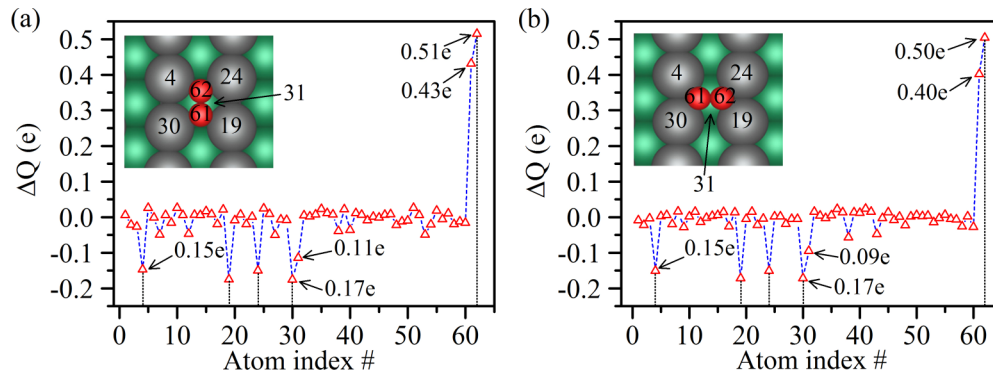


FIG. 3. (Color online) Bader analysis of charge distribution of $O_2/Ag(110)$ systems in which an O_2 molecule adsorbs in an FFH site and aligns along the (a) $[1\bar{1}0]$ and (b) $[001]$ directions. Here ΔQ represents the difference between the valence charges of isolated O and Ag atoms and the charges (calculated using Bader volumes) of each atom in the respective systems. Ag atoms (indexed as 4, 19, 24, and 30) in the top layer donate more charges than do other Ag atoms to the adsorbed O_2 molecule. Color code: Ag atoms on top layer (light gray), Ag atoms on second-from-top layer (light green), and O atoms (red).

by Gravil *et al.* [30] by more than 0.1 eV. For the $[001]$ orientation, O_2 has a substantially smaller energy difference of -0.016 eV and O-O distance (1.453 \AA) between the initial state and its dissociated O state than those for the $[1\bar{1}0]$ orientation (~ 0.3 eV and 2.057 \AA). More importantly, in the dissociation of O_2 the Ag lattice undergoes a distortion in which the Ag atoms in the topmost layer back off horizontally along the $[001]$ direction and simultaneously the Ag atoms in the second layer move upwards (by $\sim 0.5 \text{ \AA}$). Such a motion of the Ag lattice exactly matches the displacement pattern of the surface Rayleigh phonon mode (whose frequency is found to be 4.0 meV in this study and $4.2\text{--}4.4$ meV in other theoretical calculations [22,53,54] and 5.0 meV in experiments [55,56]) indicating that the dissociation of O_2 on Ag(110) is strongly coupled with a low frequency surface phonon. Considering that O_2 dissociation eventually leads to the missing-row reconstruction of Ag(110), our results suggest that the surface Rayleigh mode may undergo softening in the onset of the reconstruction. Interestingly, a similar softening of the Rayleigh mode for H-induced (2×1) reconstruction of Ni(110) was observed by Ibach and his co-workers [57].

That our calculated activation barrier for dissociation of $O_2[001]$ is smaller than that of $O_2[1\bar{1}0]$ by 0.08 eV suggests that on Ag(110) dissociation of $O_2[001]$ species is more facile than that of $O_2[1\bar{1}0]$. The favorable dissociation of O_2

along $[001]$ was also found for the case of Rh(110) [48] and Cu(110) [58]. From the discussion above, the rationale for the facile dissociation of $O_2[001]$ species on Ag(110) lies in the involvement of the surface vibrational mode and not in any noticeable difference in the net charge transfer (which is $\sim 0.9e$ from surface to the $1\pi_g^\perp$ antibonding orbital located at the Fermi level of both chemisorbed species). When O_2 lies along the $[001]$ axis it receives more boost of energy from the substrate than O_2 aligned in the $[1\bar{1}0]$ direction, because of the coupling to surface vibrations, while $O_2[1\bar{1}0]$ molecular vibrations are relatively unaffected by substrate vibrations.

B. Adsorption of atomic oxygen

In Table II we present the calculated adsorption energies of atomic oxygen in four different sites (see Fig. 5). On Ag(110), atomic oxygen prefers to adsorb in FFH, with an adsorption energy of -3.88 eV, followed very closely with adsorption at TFH, for which the adsorption energy is -3.87 eV only 10 meV less than that at FFH. Inclusion of zero-point energy slightly decreases the adsorption energy by $10\text{--}20$ meV. Our calculated adsorption energy (-3.88 eV) of O in FFH is in fact in good agreement with the previously reported value (-3.50 eV) in Ref. [31] (which does not report a value for O

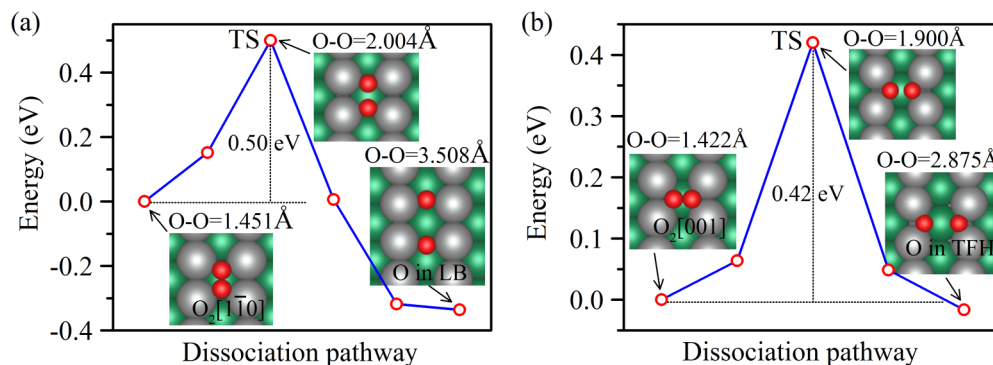


FIG. 4. (Color online) Minimum energy pathways (MEPs) for the dissociation of O_2 adsorbed in an FFH site with its orientation along the (a) $[1\bar{1}0]$ and (b) $[001]$ directions, respectively. The structures for initial states, transition states, and final states (local minima) are shown above. Color code: Ag atoms on top layer (light gray), Ag atoms on second-from-top layer (light green), and O atoms (red).

TABLE II. Adsorption energy, zero-point energy, coordination number, and charge gained by single O atom adsorbed at the four sites possible on Ag(110). $d_{\text{O-Ag}}$ indicates the distance between the O and first-neighboring Ag atoms (first and second layer). Distance between O and first-neighboring Ag atoms in second layer are given in italicized numbers.

Adsorption sites	Adsorption energy (eV)	Zero-point energy (eV)	Coordination number	$d_{\text{O-Ag}}$ (Å)	Charge gained by O (electron)
FFH	-3.88	0.022	5	2.396, 2.285	0.93
TFH	-3.87	0.033	3	2.147, 2.223	0.88
LB	-3.81	0.031	4	2.312, <i>2.203</i>	0.91
SB	-3.48	0.030	2	2.038, -	0.81

in TFH). Our results further show that the energy difference among FFH, TFH, and LB is quite small, suggesting that, at high O coverage, these sites are likely to be occupied equally. Overall, we find that SB is the least preferred adsorption site for O atom.

Bader analysis reveals (see Table II) that the net charge transfer takes place from Ag(110) to all O species, in each case increasing the O-Ag distance (distance between O and first-neighboring Ag atoms in the first layer) is proportional to the magnitude of the charge transfer. Similarly, the charge transfer to O atoms is directly proportional to the coordination number (number of bonds formed between adsorbed O and Ag atoms). This indicates that the higher the coordination number, the larger the charge transfer from Ag substrate to O atom on Ag(110). Overall, we see the following trend for these physical parameters (charge transfer, coordination number, and O-Ag bond length) of O species adsorbed in sites: FFH > LB > TFH > SB. Nevertheless, the absolute values of adsorption energy of O atoms on the four possible sites on Ag(110) shows the following trend: FFH > TFH > LB > SB.

On Ag(110), the different O species as well as the Ag atoms bonded to those O species have slightly distinct electronic structures, which would in turn differently affect their chemical activity. As shown in Fig. 6 (top panel), the p -projected density of states (p -PDOS) peak for O in FFH is slightly lower in energy than those for other oxygen atoms. This means O in FFH is more stable than other O species on Ag(110). Hence, more O in FFH will thus be available for reactions than will O at other sites. And since O at SB is the least stable species and gains slightly less charge from Ag atoms than O in other sites, it is the most prone to become mobile (relatively most transient), and thus least probable for participation in reactions. The reactivity of the Ag(110) surface is also affected by these species of O. As Fig. 6 (middle panel) displays, the electronic DOS projected onto d orbitals of Ag atoms bonded to different O species [labeled

as Ag(F), Ag(T), Ag(S), and Ag(L) corresponding to O_{FFH} , O_{TFH} , O_{SB} , and O_{LB} , respectively] indicates that the additional peaks just below the Fermi level arise from the Ag d and O p hybridization. Such states are strikingly missing on the clean Ag(110) surface (see bottom panel). Any of these O species will play an important role (approximately to the same degree) for enhancing the reactivity of Ag(110) over that of the clean surface.

Here we delineate how some electronic structure offers a clue for distinguishing the O species at the particular sites on Ag(110). In particular, our results provide insights for assigning the O species after O_2 [001] dissociation on Ag(110). Figures 7(a) and 7(b) show the charge distribution for O in three sites, FFH, TFH, and SB, as well as that of the surface Ag atoms in the O/Ag(110) system. Clearly the nearest-neighboring Ag atoms, which are bonded to the O atom, lose charge substantially. For O adsorbed in FFH, five Ag atoms [with atom indices labeled in Fig. 7(a)] offer significant contribution to the net charge transfer of $0.93e$ to the O atom, an amount similar to that transferred from Cu(001) [59] to an adsorbed O atom. This shows that not only the nearest-neighbor Ag atoms in the topmost layer of Ag(110) but also the Ag atom (marked by atom index 31) in the second layer participates in forming the O-Ag bond. Near the Fermi level (energy range from -2.5 to 0.0 eV), the atomic O p orbitals hybridize strongly with the d orbitals of the neighboring Ag atoms both in the first and second layers of Ag(110) (see Fig. 6) and play a key role in the chemisorption of atomic oxygen on Ag(110). The similar trend in electronic DOS is seen for O in the TFH site, in which case $0.88e$ charge is transferred from the Ag surface to this O species. As compared to O in FFH, O in SB gains $0.12e$ less charge from the Ag atoms, consequently p - d mixing in the latter case is relatively weaker and thereby accounting for the electronic structural difference of O in SB from O in FFH. Thus, we suggest that when O_2 aligned along the [001] direction dissociates, the dissociated O

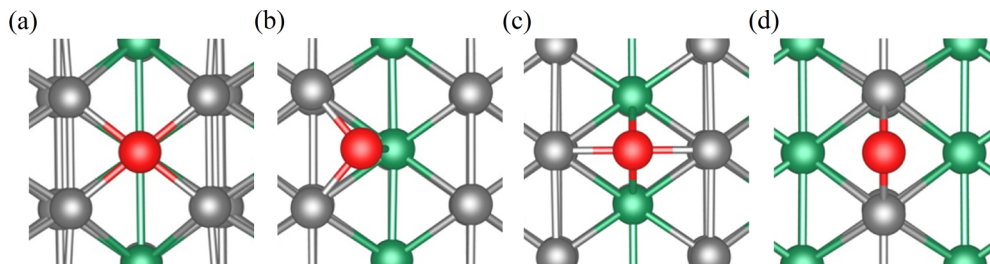


FIG. 5. (Color online) Adsorption of atomic oxygen in (a) FFH, (b) TFH, (c) LB, and (d) SB sites of Ag(110). For all of these relaxed structures of O/Ag(110), the calculated spin polarization is negligible. Color code: top-layer Ag atoms (light gray), O atoms (red), and Ag atoms in the next-to-top layer (light green).

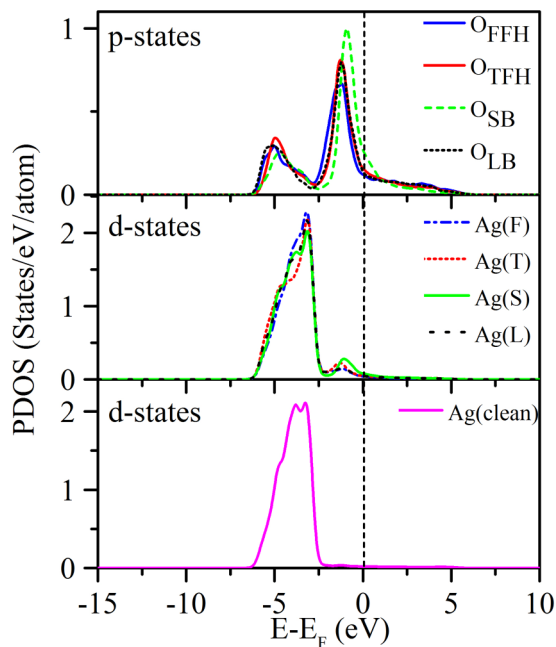


FIG. 6. (Color online) Electronic density of states projected onto the atomic p orbitals of different adsorbed O species on Ag(110) (top panel), and onto the atomic d orbitals of Ag atoms bonded to those O species (middle panel). For comparison, the bottom panel shows the d -electronic states of Ag atoms in clean Ag(110). The different O species—labeled as O_{FFH} , O_{TFH} , O_{SB} , and O_{LB} —are O adsorbed in FFH, TFH, SB, and LB sites on Ag(110), respectively. Similarly, Ag(F), Ag(T), Ag(S), and Ag(L) are Ag atoms which are bonded to corresponding O species. The Fermi level (0 eV) is indicated by the dashed line.

atoms will most likely be found at the FFH and TFH sites. The preference for thus-occupied sites of dissociated O atoms must arise from the inhomogeneous distribution of charges [see Fig. 3(b)] in adsorbed $O_2[001]$. On this point, our suggestion for the site preference of dissociated O atoms contradicts the interpretation of STM image by Hahn and Ho [29,34], who report that when O_2 aligns along the [001] direction dissociates, one O atom remains in its original FFH site and the other goes to an SB site (rather than to an TFH site close to it). Explicitly prompted by the prior theoretical conclusions [30] concerning O_2 dissociation, Hahn and Ho [29,34] conclude that the dissociation process of $O_2[001]$ consists of O-O elongation along the [001] direction, yielding the formation of O species in SB site. But our results regarding electronic structure suggest that were O species initially to settle in SB, as interpreted by Hahn and Ho, it would be likely to abruptly end up in a TFH site, since in the latter it gains more charge from the substrate than the former [cf. Figs. 7(b) and 7(c)], as a result of its higher coordination there.

C. Diffusion of atomic oxygen

In Fig. 8 we show the calculated diffusion pathways for O atom on Ag(110). Our results from CI-NEB calculations show that the diffusion of O from SB [the last configuration in Fig. 8(a)] to TFH [the third configuration in Fig. 8(a)] or FFH (the first configuration in Fig. 8(a) along the [001] direction)

confronts no barrier at all. This means that O in SB can spontaneously diffuse to TFH, indicating that the adsorption of O in SB is quite unstable in the presence of external perturbation. In contrast, the diffusion of O from SB via FFH to another SB along the [001] direction needs to overcome a barrier of 0.42 eV [Fig. 8(a)]. In particular, an O atom in TFH has to overcome a barrier of 0.39 eV in order to diffuse from TFH to SB. The small barrier of 0.03 eV for diffusion from TFH [the third configuration in Fig. 8(a)] to FFH [the first configuration in Fig. 8(a)], the lowest potential energy of all sites, is an indication that the preferred site for O adsorption on Ag(110) is FFH, followed by TFH. Now the energy barrier for the diffusion of O from FFH to the next nearest FFH along $[1\bar{1}0]$ is only 0.072 eV [Fig. 8(b)]. Moreover, our results show that O in LB is in a “local minimum” state. This O atom in LB needs to overcome a very small barrier of 0.045 eV to diffuse from LB to FFH. Overall, an O atom can quite easily diffuse from an FFH site to another FFH site along the $[1\bar{1}0]$ direction. But O diffusion is not so easy from one FFH to another FFH site along an [001] axis, as it needs to overcome an energy barrier of 0.42 eV.

Let us now compare and contrast our DFT results for the diffusion of O species with the experimental results [29] in a way that, while providing the rationale for the complex diffusion pathway of O species, will resolve certain issues that arise in the authors’ interpretation of their STM images. Our results show that, to diffuse from one SB site to another SB along the $[1\bar{1}0]$ direction, O needs to overcome an energy barrier of 1.08 eV, which is higher than the barrier of 0.42 eV along the [001], thus indicating that O should preferentially diffuse along the [001]. However, Hahn and Ho [29] not only maintain that O diffuses from an SB site to another SB either along [001] or along $[1\bar{1}0]$ but infer from this that O diffusion from a SB to another SB is easier than O diffusion from a SB to FFH. Our calculated potential energy surface (PES) profile [Fig. 8(a)], however, indicates that O species can easily diffuse from an SB to an FFH site without experiencing any barrier. Their observation that “ O_{sb} atoms always diffused to other short-bridge sites, even if they could diffuse along either the [001] or $[1\bar{1}0]$ direction” appears to derive in turn from their interpretation of the STM image in their Fig. 1, and in particular from “the grid lines drawn through the Ag surface atoms,” which lead them to assign the bright protrusion on the STM images reported for O atom at low coverage on Ag(110) to O in SB. From their remark that the average atomic separation induced by a negative voltage pulse is 11.7 Å, about 2.9 times the lattice spacing along the [001] direction, we can infer that the lattice constant they employed in constructing the imposed grid is 4.034 Å—somewhat smaller than the experimental value of 4.086 Å reported in Ref. [38] and our calculated value of 4.147 Å. (We are not told in Ref. [29] what the source is for the values employed in that study.) Note that if the grid Hahn and Ho used as their lens for assigning the position of the dissociated O atom had been only slightly larger than the one they used, that atom’s image would have appeared to sit in (or at least closer to) the TFH site immediately adjacent to the SB site.

In any case, our DFT calculations suggest that O cannot exist in an SB site as residual stable species. It might be supposed that this species is stabilized by other O species

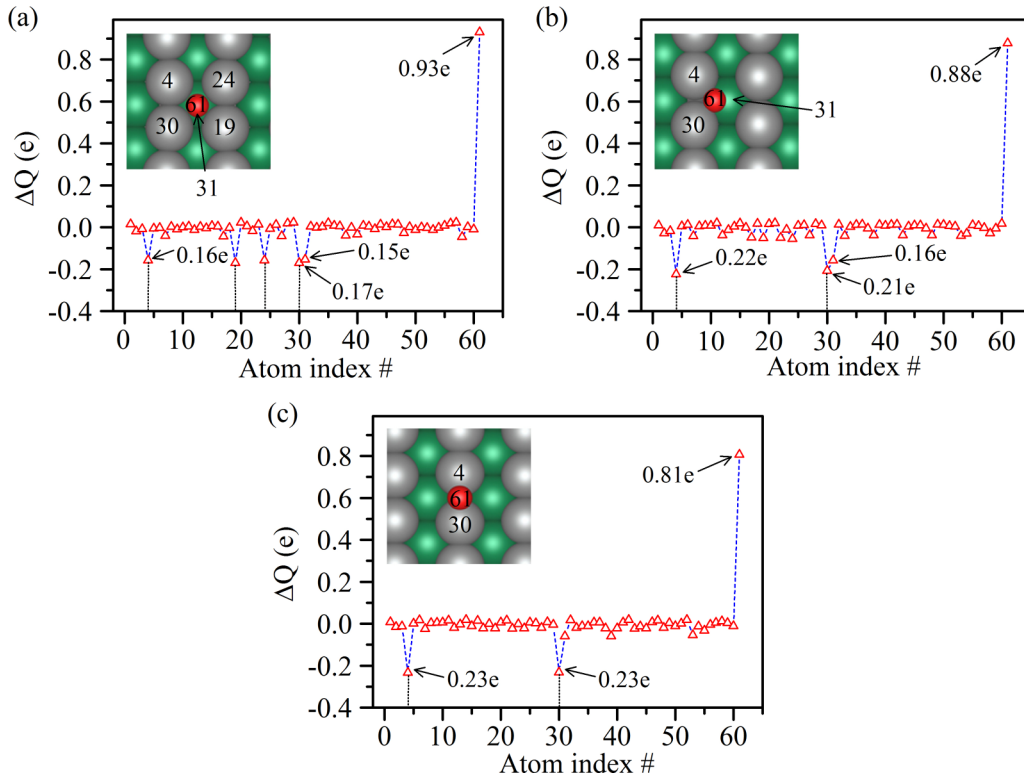


FIG. 7. (Color online) Bader analysis of charge distribution of O/Ag(110) systems in which atomic O adsorbs in (a) FFH, (b) TFH, and (c) SB sites of Ag(110). Here ΔQ represents the difference between valence charges and charges (calculated using Bader volumes) of each atom in the respective systems. Ag atoms (indexed as 4, 19, 24, 30, and 31 in the top layer) donate more charges than other Ag atoms to the adsorbed O. Color code: Ag atoms on top layer (light gray), Ag atoms on second-from-top layer (light green), and O atoms (red).

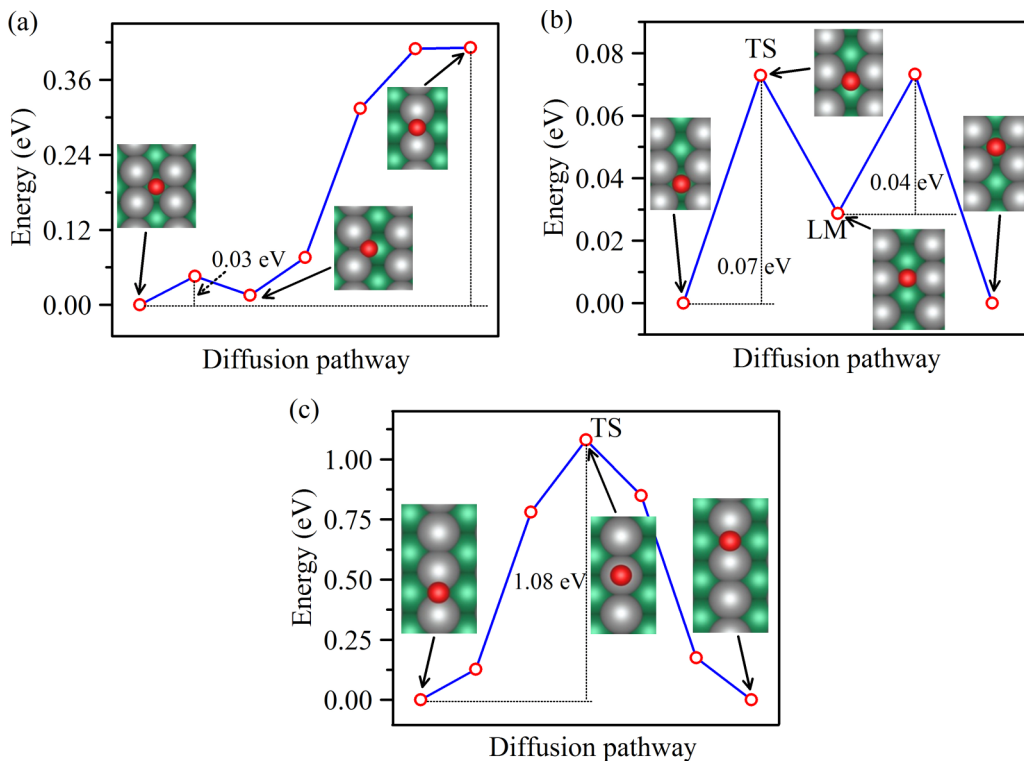


FIG. 8. (Color online) Diffusion of atomic oxygen: (a) from FFH to SB along $[001]$ direction, (b) from FFH to FFH along $[1\bar{1}0]$ direction, and (c) from SB to SB along the $[1\bar{1}0]$ direction. The initial states, transition states, and final states are also shown. Color code: Ag atoms on top layer (light gray), O atoms (red), and Ag atoms on second top layer (light green).

TABLE III. Vibrational frequencies of an O atom adsorbed at four possible sites on Ag(110), after relaxation of both adsorbate and substrate. For each site of O on Ag(110), we give in parentheses the frequencies calculated with only O allowed to vibrate, and the Ag substrate is frozen.

Vibrational modes	FFH (meV)	TFH (meV)	SB (meV)	LB (meV)	Expt. (meV)
O-Ag stretching	38(35)	44(39)	54(51)	43(33)	40.5, ^a 39.1, ^b 40.0 ^c
Frustrated translation along the $[1\bar{1}0]$ direction	21(19)	41(38)	51(47)	35(30)	
Frustrated translation along the $[001]$ direction	20(13)	33(23)	-10(-7)	22(19)	

^aReference [17] EELS measurements (not site specific).

^bReference [60] EELS measurements (not site specific).

^cReference [61] EELS measurements (not site specific).

via *long-range interactions* that could be mediated by Ag substrate. But on the basis of our DFT results, we instead suggest that the O species Hahn and Ho report as stabilized in SB may in fact be O stabilized in TFH. The following facts should be taken into account: (i) O species in TFH is lower in energy than O at SB by 0.39 eV; (ii) the PES is without energy barrier—strongly downhill—for the diffusion from an SB to an FFH site; (iii) TFH and SB sites are very, very close to each other (~ 1.265 Å—less than the average O-Ag distance). Thus, it was quite challenging to distinguish O in TFH from O in SB in the STM images reported in Refs. [29,34].

D. Vibration of oxygen on Ag(110)

1. Vibration of atomic oxygen

In Table III we present the results of our calculation of vibrational frequencies of atomic oxygen adsorbed in four different sites on Ag(110), and compare them with those obtained by experiments. The stretching mode of an O atom in FFH (the preferred adsorption site at low coverage $[1/12]$) against the substrate is found to have a frequency of 38 meV. All experimental measurements of vibrations of O on Ag(110) were carried out by EELS, and, while all of these studies agree in attributing them to the stretching mode (we take up one partial exception, below), none of these studies attempted to attribute detected vibrations to any particular adsorption site. Note, though, that not only is one of these (39.1 meV, Ref. [60]) quite closely in agreement with our calculated value (38 meV) for O in FFH but that even the other two reported values (40 meV, Ref. [61]) (we take up the second value in this study below); (40.5 meV, Ref. [17]) are closer to our calculated value for that species of O than even to our next-highest calculated value (43 meV, for O in LB). This suggests that the vibrational-frequency values discussed in the experimental studies primarily registered what our calculations found for O in FFH, which as our calculations for adsorption energy (Sec. III B) indicate, is the preferred adsorption site for O on Ag(110). Indeed, the fact that the experimental values were slightly higher than our calculated value for O in FFH may reflect the contribution to the frequency in real situations of lesser quantities of O in the less-favored sites: our calculations of the vibrational frequencies for the same mode (stretching of O against the substrate) of O in TFH, SB, and LB turn out to be 44, 54, and 43 meV, respectively—all of which are higher than that of O in FFH.

Note, too, that the O atom in SB has one negative mode (-10 meV), and that this is the frustrated translation mode (swinging motion along the $[001]$ axis). Together these facts

indicate not only that O in SB is unstable but that its oscillation directs the O atom towards TFH, a downhill direction in the potential energy surface (PES). The character of this mode is another fact that suggests that Hahn and Ho's interpretation of their STM image as displaying O in SB is not realistic.

Interestingly, one of the experimental studies [61] indicates an additional vibration at 54 meV (not taken up in discussion), which coincides with our calculated frequency of 54 meV for O species in SB. If this vibration really derives from O species in SB, then such species somehow must have been stabilized by other O species on Ag(110) before the measurements were carried out. Such a stabilization afforded by other O species on Ag(110) may occur only at higher O coverage than we examine in the present study. This is a possibility that warrants further investigation.

2. Vibration of O₂

The O-O intramolecular vibrational frequency of gas-phase O₂ turns out to be 194 meV, in good agreement with the experiment (196 meV). Upon adsorption, the vibrational frequency is affected by the O₂-Ag interaction and thus depends on the adsorption site and molecular orientation. We illustrate the displacements of the vibrational modes of O₂ on Ag(110) in Fig. 9. In Table IV we present the vibrational frequencies of O₂ adsorbed in four different sites with the molecular axis aligned either along the $[001]$ or $[1\bar{1}0]$ direction. The highest-frequency mode for all sites and orientations of O₂ is O-O intramolecular stretching (denoted as mode_1). Note that in this mode there is no difference for O₂ $[1\bar{1}0]$ between the frequencies in the frozen and unfrozen configurations. In contrast, for O₂ $[001]$, the frequency is higher when both the molecule and substrate are allowed to vibrate than when the substrate is frozen. This indicates that O₂ gains energy from the Ag(110) substrate only when it adsorbs aligning along the $[001]$ axis. This extra energy helps explain why the dissociation barrier for O₂ $[001]$ is lower than it is for O₂ $[1\bar{1}0]$.

Mode_1 of O₂ $[1\bar{1}0]$ has the frequency of 92 meV, slightly higher than experiments [17,61]. Mode_2, the frustrated rotation around the z axis, has a frequency of 40 meV. As such, this mode can induce the rotation of O₂ from $[1\bar{1}0]$ to $[001]$ direction. Mode_3 has the frequency of 28 meV assigned as the frustrated rotation around the x axis.

For the O₂ $[001]$ species, we find that mode_1 has the frequency of 84 meV (in the frozen configuration) and of 96 meV (in the unfrozen configuration). Mode_2 of O₂ $[001]$ has the frequency of 38 meV, of which eigenvectors lead to yield the frustrated rotation around the z axis in the xy plane.

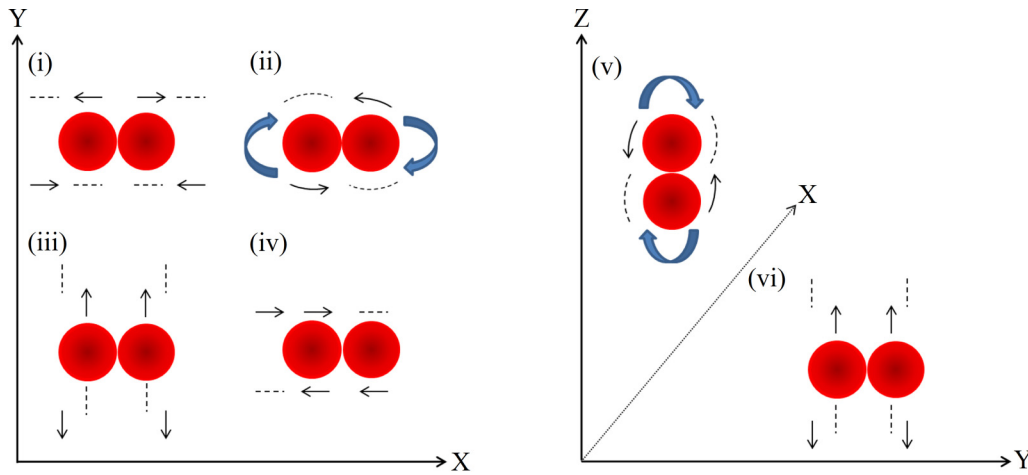


FIG. 9. (Color online) Vibrational modes of O_2 on $Ag(110)$: (i) *Intramolecular stretching*, in which O atoms vibrate opposite to each other. (ii) *Frustrated rotation* around the z axis in an xy plane. (iii) *Translational mode* associated with the oscillation of O_2 along the $[1\bar{1}0]$ or Y direction. (iv) *Translational mode* associated with the oscillation of O_2 along $[001]$ or X direction. (v) *Frustrated rotation* around the x axis in the yz plane. (vi) *Stretching mode* of O_2 against the $Ag(110)$ substrate. The directions of oscillation are indicated by arrows. In Table IV “mode_1” indicates intramolecular stretching, mode_2 and mode_3 represent either frustrated rotational (fr) or frustrated translational (ft) or molecule-substrate (ms) stretching vibrational modes of O_2 , as indicated in Table IV and described in the text.

This mode can induce the rotation of adsorbed O_2 from the $[001]$ direction to the $[1\bar{1}0]$, energetically favorable to its reverse orientation since the adsorption energy of $O_2[1\bar{1}0]$ is lower than that of $O_2[001]$. Mode_3 of $O_2[001]$ has the frequency of 32 meV, arising from frustrated rotation around the x axis on the yz plane. This frustrated rotational mode can induce the O_2 to dissociate along the $[001]$ axis. Upon dissociation, the dissociated O atoms could initially adsorb in TFH sites but eventually diffuse to FFH—the favored adsorption site at our low coverage. However, either rotation or dissociation of $O_2[001]$ species depends upon the favorable physical conditions. One previous theoretical study [62] shows that, in FFH, the frequency of $O_2[001]$ and $O_2[1\bar{1}0]$ are 100 and 95 meV, respectively. The other [63] reports that the vibrational frequencies of $O_2[001]$ and $O_2[1\bar{1}0]$ in FFH are 103 and 101 meV, respectively. Thus, our calculated vibrational frequencies (96 and 92 meV for $O_2[001]$ and $O_2[1\bar{1}0]$, respectively) are in reasonable agreement with values obtained in the only other theoretical studies heretofore [62,63]: the respective frequencies vary slightly in range, but in all three studies the frequency for $O_2[001]$ is slightly higher than that for $O_2[1\bar{1}0]$.

For the LB site, the mode_1 of $O_2[1\bar{1}0]$ has a vibrational frequency of 92 meV (in both frozen and unfrozen configurations) similar to that of $O_2[1\bar{1}0]$ in FFH site. Mode_2 has a frequency of 30 meV, of which corresponding eigenvectors lead to yield the frustrated rotation around the x axis in the yz plane. Mode_3 has a frequency of 23 meV generated by the O_2 -Ag stretching. On the other hand, for $O_2[001]$ in LB, the mode_1 frequency is found to be 111 meV (in the frozen configuration) and 126 meV (in the unfrozen configuration), the latter of which is in reasonable agreement with the only previous theoretical calculations [63]—we assume that the value reported there (119 meV) is for the configuration in which both the molecule and the substrate were allowed to vibrate. Mode_2 has a frequency of 40 meV, pertaining to the frustrated rotation around the y axis in the xz plane. Mode_3 has the frequency of 26 meV, arising from O_2 -Ag stretching.

For O_2 in SB, the mode_1 frequency of $O_2[001]$ turns out to be 94 meV (in the frozen configuration) and 108 meV (in the unfrozen configuration). Mode_2 has a frequency of 23 meV, pertaining to the frustrated O_2 -Ag stretching. Mode_3 has a frequency of 22 meV, of which corresponding eigenvectors lead to yield the swinging-to-and-fro motion (translational

TABLE IV. Vibrational frequencies of an O_2 molecule adsorbed at four possible sites of $Ag(110)$. For each site of and orientation of O_2 on $Ag(110)$, we give in parentheses the frequencies calculated with only O_2 allowed to vibrate, and the Ag substrate is frozen.

Vibrational modes	FFH (meV)		LB (meV)		SB (meV)		TOP (meV)		Expt. (meV)
	[001]	$[1\bar{1}0]$	[001]	$[1\bar{1}0]$	[001]	$[1\bar{1}0]$	[001]	$[1\bar{1}0]$	
Mode_1	96(84)	92(92)	126(111)	92(92)	108(94)	127(127)	136(119)	135(135)	80 ^a , 85 ^b
Mode_2	40(36)	38(38)	44(40)	30(30)	27(23)	42(41)	25(22)	23(20)	
	fr	fr	fr	fr	fr	ms	ms	ms	
Mode_3	32(30)	28(27)	28(26)	23(21)	25(22)	32(30)	14(11)	13(8)	
	fr	fr	ms	ms	ms	ft	fr	fr	

^aReferences [17,61].

^bReference [17].

mode) along the $[1\bar{1}0]$ axis. In contrast, we find the intramolecular stretching frequency of $O_2[1\bar{1}0]$ is 127 meV in both frozen and unfrozen configuration. A theoretical study [62] reports that, for both SB and LB sites, the intramolecular stretching frequency of $O_2[1\bar{1}0]$ is identical (i.e., 141 meV for both sites)—higher than our calculated frequency (127 meV) for $O_2[1\bar{1}0]$ in SB. We find mode_2 has the frequency of 42 meV, pertaining to the frustrated rotation around the x axis in the yz plane and mode_3 has the frequency of 32 meV, of which corresponding eigenvectors lead to yield the O_2 -Ag stretching.

For $O_2[1\bar{1}0]$ at TP, we find mode_1 has the frequency of 134 meV (in the frozen configuration) and 135 meV (in the unfrozen configuration), mode_2 has the frequency of 20 meV (in the frozen configuration) but 23 meV (in the unfrozen configuration), of which corresponding eigenvectors lead to yield the O_2 -Ag stretching, and mode_3 has the frequency of 13 meV, pertaining to the frustrated rotation around the x axis in the yz plane. The other modes of $O_2[001]$ at TP are negative (i.e., unstable). We have already shown (Sec. III A1) that, energetically, $O_2[001]$ at TP is the most unstable species of all.

Overall, our results show that the highest-frequency mode of adsorbed O_2 on Ag(110) in all cases (regardless of orientation and adsorption site) corresponds to its O-O intramolecular stretching, which fosters its dissociation along either the $[001]$ or the $[1\bar{1}0]$ direction, depending upon the initial orientation. In most cases, the second-highest frequency mode of O_2 corresponds to the frustrated rotational mode, which may induce rotation of O_2 .

Furthermore, our results show that while the O-O intramolecular stretching frequency of $O_2[1\bar{1}0]$ is not affected when, in the calculations, the Ag substrate atoms are allowed to vibrate, that of $O_2[001]$ is substantially affected by the substrate atomic displacements—up to 10–12 meV. Our calculations thus indicate that the intramolecular stretching frequency of $O_2[001]$ is strongly coupled with the substrate vibration so that dissociation of $O_2[001]$ is more strongly affected by substrate vibrations than is $O_2[1\bar{1}0]$. The rationale for this directional difference of O_2 coupling with substrate vibration may not be so difficult to understand: As $O_2[001]$ has shorter O-Ag and O-O bond lengths, a change in Ag position (i.e., Ag ionic-core motion) is likely to induce a greater force on its O atoms than those constituting $O_2[1\bar{1}0]$. As discussed at the end of Sec. III A2, O_2 dissociation along the $[001]$ axis is coupled with a surface phonon mode (4.0–5.0 meV). Since this surface phonon can be activated at relatively low temperatures, activation of O_2 dissociation along the $[001]$ direction is facilitated at low temperatures.

E. Evaluating the discrepancy between our results and those of Gravil *et al.* [1]

Even though both Gravil *et al.* [30] and we employ DFT within the GGA approximation in studying adsorption and dissociation of O_2 on Ag(110), our results for these physical processes are quite different. As to adsorption, though our results agree that the preferred site is FFH, our calculations show that $O_2[1\bar{1}0]$ is more favorable than $O_2[001]$ with an energy difference of 40 meV, whereas Gravil *et al.* find that $O_2[001]$ is more favorable than $O_2[1\bar{1}0]$ with the same

energy difference. As to dissociation, our calculated values of activation barriers for $O_2[1\bar{1}0]$ and $O_2[001]$ dissociations are, respectively, 0.50 and 0.42 eV, which turn out to be smaller than those (0.62 and 0.76 eV, respectively) calculated by Gravil *et al.* [30] by more than 0.1 eV.

Between their study and ours, there are several methodological distinct features that may partly be the sources of the discrepancies in results. In addition, there are certain lines of evidence supporting our results that were not available to them. Part of the discrepancies in both aspects may be due to the use of different flavors of functional as well as pseudopotential. The PAW method for generating the pseudopotential [37,64] is now generally thought to be more reliable than the norm-conserving pseudopotential [65,66] used by Gravil *et al.* [30]. (Whether the PBE functional [36] is superior to the PW functional [67] is perhaps a more debatable issue. And whether there are hybrid DFT functionals that would lead to yet another conclusion is not an argument that we are in a position to comment here.) Note, too, that our DFT calculations exploit a finer k -point grid for sampling the BZ (9 points vs 4), a lattice constant (4.147 vs 4.190 Å) for constructing the surface supercell closer to the experimental value (4.086 Å) [38], and a more stringent criterion for force convergence (0.01 vs 0.1 eV/Å), than Gravil *et al.* use. Moreover, computational resources have greatly increased in the interval between the two studies, enabling us to use a 3×4 unit cell instead of a 3×2 .

It is worth mentioning that our DFT calculations, indicating $[1\bar{1}0]$ as the favorable orientation of an adsorbed O_2 , are supported by two lines of theoretical evidence not accessible to Gravil *et al.* [30]. First, they are in a line with MD simulations [17] carried out for determining the chemisorbed O_2 species from physisorbed O_2 . Second, as we have already shown, on Ag(110) the favorability of O_2 orientation along $[1\bar{1}0]$ over that along $[001]$ direction is corroborated by the lower O-O stretching frequency of 92 meV (for $O_2[1\bar{1}0]$) than the frequency of 96 meV (for $O_2[001]$). In Gravil *et al.*, no analysis of vibrational frequency was carried out, and so one could argue on the validity of their results.

The discrepancy in our results concerning O_2 dissociation on Ag(110) and those of Gravil *et al.* [30] may be due in part to additional methodological difference. That they obtain their values for the dissociation barrier from PES indicates that they are estimating the value for the incoming molecule. Our calculations yield the dissociation barrier for the molecule as already adsorbed on the surface. In doing so, we use the now-standard CI-NEB method (introduced only in 2000 [43]), Gravil *et al.* do not specify the method they used for calculating the dissociation barrier. One has therefore (today) to guess what this might have been. Though the original nudged elastic band (NEB) method was available in 1996, it would be surprising if they had used it without citing the original reference. Moreover, at that time NEB was probably not implemented in many DFT codes. One possibility is thus that they did the estimation “by a hand,” i.e., by comparing the minimum and saddle point energies that are evaluated after few steps by just relaxing the dissociating O_2 on Ag(110) in the constrained geometry. This method allows dissociating O_2 to stretch along its axis, by keeping its other two coordinates fixed, in contrast to the NEB method that includes all degrees

of freedom (i.e., including along the axis of dissociation) during relaxation of the O_2 . Hence, one would expect our calculated activation barriers to be more reliable than theirs. Our calculated barriers are in a line with what our vibrational frequency results imply is at least an important part of the underlying mechanism: unlike $O_2[1\bar{1}0]$, the $O_2[001]$ species gains vibrational energy from the substrate; as a result, this species confronts a lower activation barrier for dissociation along the $[001]$ direction than $O_2[1\bar{1}0]$ does along $[1\bar{1}0]$. That is why on Ag(110) $O_2[001]$ dissociation is more facile than $O_2[1\bar{1}0]$ dissociation.

We note in passing that we have calculated the diffusion paths for O atoms, an issue Gravil *et al.* [30] do not address. Our detailed analysis of the diffusion mechanism of dissociated O atoms helps resolve some associated issues introduced by the physical interpretation of STM images measured by Hahn and Ho [29,34]. Indeed, our analysis takes a step forward by providing the complete picture of diffusion of O atoms that lead to not only fundamental insights in understanding the reactivity of Ag(110) but also the direction for accurate description of future experimental observations.

F. Evaluating the discrepancy between our results and those of Hahn and Ho [29,34]

Part of Hahn and Ho's interpretation about the diffusion of oxygen on Ag(110) arises from the above theoretical conclusion of Gravil *et al.* [30] about the dissociation of O_2 , but this reliance enters their analysis only at a later stage. They are puzzled by the unexpected result, from reading of their STM image, that while one of the dissociated O atoms remains in its original FFH site, the other ends up on an SB site, and turn to Gravil's theoretical study of a possible mechanism by which this could take place: taking for granted (from the latter) that the dissociation barrier for $O_2[001]$ is higher along the $[001]$ direction than along the $[1\bar{1}0]$, they infer that "the dissociation process involves a larger extension of the O-O bond along the $[001]$, enabling the formation of the O_{sb} species." But, as we have argued in Sec. III C, this view of the relative dissociation barriers along the two possible directions is different from ours.

According to Hahn and Ho, O atoms diffuse easily from one SB to another SB, regardless of the direction, whether $[001]$ or $[1\bar{1}0]$. But if this were the case, O at SB would have to confront a higher barrier for diffusing to a FFH site than for diffusing to an SB site. As we have shown, however, while there is no barrier for O to diffuse from SB to FFH, the barrier for diffusion from one SB to another SB along $[1\bar{1}0]$ and along $[001]$ are 1.08 and 0.42 eV, respectively. This is further evidenced by our vibrational frequency calculation, which shows that O-Ag stretching frequency of O at SB is higher than that of other O species (in FFH, TFH, and LB) on Ag(110). In addition, the emergence of one imaginary mode of O at SB reinforces our prediction that this species is not stable. Thus, our results suggest that O at SB, as inferred by Hahn and Ho, is not realistic. Rather, this O species they so identified would more likely reside in TFH, for the following reasons: (i) O in TFH is lower in total energy than O at SB by 0.39 eV; (ii) the PES for diffusion from an SB to a TFH site is strongly downhill (in fact, without energy barrier) while that for diffusion in the

opposite direction is, in comparison, uphill (0.39 eV); (iii) O at SB has one imaginary frequency; (iv) TFH and SB sites are very close to each other ($\sim 1.265 \text{ \AA}$ —less even than the average O-Ag distance) and thus easy to confuse, particularly if one's estimation of the lattice constant is even slightly too small.

IV. CONCLUSIONS

We have performed DFT calculations for the adsorption, dissociation, diffusion, and vibration of oxygen on Ag(110). Our calculations show that the fourfold-hollow (FFH) site is the preferred adsorption site for O_2 , and that O_2 in FFH oriented along the $[1\bar{1}0]$ direction is slightly more favorable than O_2 oriented along the $[001]$. By weakening the O-O bond, the net charge transfer of $\sim 0.9e$ (as calculated using Bader's approach) from Ag(110) to the antibonding ($2\pi^*$) orbital of adsorbed O_2 , in fact, facilitates its dissociation on Ag(110). However, the elongation of the O-O bond is not directly correlated to the activation barrier for O_2 dissociation. Rather, the surface corrugation, the substrate vibration, and the preference of the structural distortions on Ag(110) all have partial effects on the interaction experienced by dissociated O atoms, and hence on the activation barriers. Our vibrational frequency analysis exhibits that, for O_2 species aligned along the $[001]$ direction, the O-O stretching mode is strongly coupled with the substrate vibration and hence the dissociation of these species is induced by the substrate vibration. On the basis of our CI-NEB calculations, we find that dissociation of O_2 along the $[001]$ direction (with a barrier of 0.42 eV) is more favorable than that of O_2 along the $[1\bar{1}0]$ direction (with a barrier of 0.50 eV). Since $O_2[001]$ species, unlike the $O_2[1\bar{1}0]$, gains vibrational energy from the substrate, so the dissociation of $O_2[001]$ turns out to be more facile than that of $O_2[1\bar{1}0]$.

Recall that the experimental study reported in Refs. [29,34] proposes that the diffusion path of O atom is from one SB site to another SB on Ag(110), along either the $[001]$ or the $[1\bar{1}0]$ direction. The results of our DFT calculations imply that such a path is not realistic. They provide four lines of evidence that the diffusion path for O on Ag(110) is quite different (and more complex). (i) At low coverage (excluding the complex features of dissociated O atoms), the adsorption energy of O in an SB site is higher than that of O in any other available site. This implies that O will not follow a diffusion path from one SB site to another: with such a high adsorption energy, it is most likely neither to start from nor to end in an SB site. (ii) For O species at an SB site, there exists one negative vibrational frequency mode, which induces the oscillation of this species towards the minimum potential energy site—either TFH or (slightly favored, by 0.01 eV) FFH. (iii) The activation barrier for diffusing O from an FFH site to the next nearest FFH site along the $[1\bar{1}0]$ direction is ~ 0.07 eV, which is far smaller (5.7 times smaller) than the barrier for diffusing from an SB to another SB, regardless of the direction. (iv) O species in an SB site prefers to diffuse along the $[001]$ direction rather than along the $[1\bar{1}0]$, because the barrier for so diffusing is 2.7 times lower than for diffusing from one SB to another SB along the $[1\bar{1}0]$ direction. Instead, the most likely diffusion path of O from an SB site is to a TFH site, owing to the downhill potential along this path. (The fact that a TFH site is

geometrically very close to an SB site makes it quite difficult for experiment to resolve clearly the difference between the two.)

Still, although we resolve some issues regarding the complex diffusion path of atomic oxygen on Ag(110) using standard CI-NEB calculations (which presuppose very low T), the limitation of DFT does not allow one to incorporate the effect of excited states, as would be necessary to establish whether or not under higher temperature conditions it is possible for O to stabilize at an SB site. To determine this, one would need to resort to some advanced theoretical approaches, such as time-dependent DFT (TDDFT) which is beyond the scope of this work.

Moreover, although our DFT results provide some physical insights important for understanding the physical processes of adsorption, dissociation, diffusion, and vibration of oxygen on Ag(110) and thus for determining the active oxygen species on Ag(110) for various oxidation reactions, further investigation is required to pinpoint the role, in these reactions, of the

additional d -electronic state just below the Fermi level, since this state would turn out to be important for the catalytic significance of oxidation reactions on Ag(110).

ACKNOWLEDGMENTS

This work was partly supported by the U.S. National Science Foundation under Grant No. CHE-1310327. We thank Mario Rocca and Jagriti Pal for the fruitful discussions of our results. Our sincere thanks go to Lyman Baker for critical reading of the manuscript, and for providing many insightful comments that have helped us rationalize our results. We also acknowledge the STOKES Advanced Research Computing Center at the University of Central Florida, the Texas Advanced Computing Center (TACC), the National Energy Research Scientific Computing Center (NERSC), and the Center for Nanoscale Materials (CNM) of the Argonne National Laboratory for providing computational resources for accomplishing this work.

-
- [1] W.-L. Dai, Q. Liu, Y. Cao, and J.-F. Deng, *Appl. Catal. A: General* **175**, 83 (1998).
- [2] L. Savio, A. Gerbi, L. Vattuone, M. Rocca, F. Vecchiocattivi, D. Cappelletti, and F. Pirani, *Chem. Phys. Lett.* **404**, 336 (2005).
- [3] J. G. Serafin, A. C. Liu, and S. R. Seyedmonir, *J. Mol. Catal. A: Chem.* **131**, 157 (1998).
- [4] C. T. Campbell and M. T. Paffett, *Surf. Sci.* **139**, 396 (1984).
- [5] L. Vattuone, M. Rocca, C. Boragno, and U. Valbusa, *J. Chem. Phys.* **101**, 713 (1994).
- [6] P. A. Gravil, J. A. White, and D. M. Bird, *Surf. Sci.* **352**, 248 (1996).
- [7] D. A. Outka, J. Stöhr, W. Jark, P. Stevens, J. Solomon, and R. J. Madix, *Phys. Rev. B* **35**, 4119 (1987).
- [8] U. Burghaus and H. Conrad, *Surf. Sci.* **364**, 109 (1996).
- [9] J. R. Hahn and W. Ho, *Phys. Rev. Lett.* **87**, 166102 (2001).
- [10] M. A. Barteau and R. J. Madix, *J. Am. Chem. Soc.* **105**, 344 (1983).
- [11] J. V. Barth and T. Zambelli, *Surf. Sci.* **513**, 359 (2002).
- [12] J. V. Barth, T. Zambelli, J. Wintterlin, and G. Ertl, *Chem. Phys. Lett.* **270**, 152 (1997).
- [13] Y. Kuk and L. C. Feldman, *Phys. Rev. B* **30**, 5811 (1984).
- [14] B. W. Busch and T. Gustafsson, *Surf. Sci.* **407**, 7 (1998).
- [15] J.-K. Hansen, J. Bremer, and O. Hunderi, *Surf. Sci.* **418**, L58 (1998).
- [16] K. C. Prince, G. Paolucci, and A. M. Bradshaw, *Surf. Sci.* **175**, 101 (1986).
- [17] F. Bartolucci, R. Franchy, J. C. Barnard, and R. E. Palmer, *Phys. Rev. Lett.* **80**, 5224 (1998).
- [18] L. Vattuone, P. Gambardella, U. Valbusa, and M. Rocca, *Surf. Sci.* **377–379**, 671 (1997).
- [19] L. Vattuone, M. Rocca, P. Restelli, M. Pupo, C. Boragno, and U. Valbusa, *Phys. Rev. B* **49**, 5113 (1994).
- [20] M. A. Barteau and R. J. Madix, *J. Chem. Phys.* **74**, 4144 (1981).
- [21] W. W. Pai, N. C. Bartelt, M. R. Peng, and J. E. Reutt-Robey, *Surf. Sci.* **330**, L679 (1995).
- [22] L. Yang, T. S. Rahman, G. Bracco, and R. Tatarek, *Phys. Rev. B* **40**, 12271 (1989).
- [23] M. Canepa, P. Cantini, F. Fossa, L. Mattera, and S. Terreni, *Phys. Rev. B* **47**, 15823 (1993).
- [24] D. J. Coulman, J. Wintterlin, R. J. Behm, and G. Ertl, *Phys. Rev. Lett.* **64**, 1761 (1990).
- [25] S. R. Parkin, H. C. Zeng, M. Y. Zhou, and K. A. R. Mitchell, *Phys. Rev. B* **41**, 5432 (1990).
- [26] V. Pouthier, C. Ramseyer, C. Girardet, P. Zeppenfeld, V. Diercks, and R. Halmer, *Phys. Rev. B* **58**, 9998 (1998).
- [27] X. Duan, O. Warschkow, A. Soon, B. Delley, and C. Stampfl, *Phys. Rev. B* **81**, 075430 (2010).
- [28] P. Cabrera-Sanfelix, C. Lin, A. Arnau, and D. Sánchez-Portal, *J. Phys.: Condens. Matter* **25**, 135003 (2013).
- [29] J. R. Hahn and W. Ho, *J. Chem. Phys.* **123**, 214702 (2005).
- [30] P. A. Gravil, D. M. Bird, and J. A. White, *Phys. Rev. Lett.* **77**, 3933 (1996).
- [31] F. E. Olsson, N. Lorente, and M. Persson, *Surf. Sci.* **522**, L27 (2003).
- [32] P. J. Van Den Hoek and E. J. Baerends, *Surf. Sci.* **221**, L791 (1989).
- [33] S. Monturet, M. Alducin, and N. Lorente, *Phys. Rev. B* **82**, 085447 (2010).
- [34] J. R. Hahn and W. Ho, *J. Chem. Phys.* **122**, 244704 (2005).
- [35] G. Kresse and J. Furthmüller, *Comp. Mater. Sci.* **6**, 15 (1996).
- [36] J. P. Perdew, K. Burke, and M. Ernzerhof, *Phys. Rev. Lett.* **77**, 3865 (1996).
- [37] P. E. Blöchl, *Phys. Rev. B* **50**, 17953 (1994).
- [38] P. Walker and W. H. Tarn, *CRC Handbook of Metal Etchants* (CRC, New York, 1990).
- [39] J. D. Pack and H. J. Monkhorst, *Phys. Rev. B* **16**, 1748 (1977).
- [40] M. Methfessel and A. T. Paxton, *Phys. Rev. B* **40**, 3616 (1989).
- [41] W. H. Press, S. A. Teukolsky, W. T. Vetterling, and B. P. Flannery, *Numerical Recipes* (Cambridge University Press, New York, 2007).

- [42] E. Polak, *Computational Methods in Optimization* (Academic, New York, 1971).
- [43] G. Henkelman, B. P. Uberuaga, and H. Jonsson, *J. Chem. Phys.* **113**, 9901 (2000).
- [44] R. F. W. Bader, *Atoms in Molecules: A Quantum Theory* (Oxford University Press, New York, 1990).
- [45] G. Henkelman, A. Arnaldsson, and H. Jónsson, *Comp. Mater. Sci.* **36**, 354 (2006).
- [46] S. Y. Liem, J. H. R. Clarke, and G. Kresse, *Comp. Mater. Sci.* **17**, 133 (2000).
- [47] B. G. Briner, M. Doering, H. P. Rust, and A. M. Bradshaw, *Phys. Rev. Lett.* **78**, 1516 (1997).
- [48] S. W. Hla, P. Lacovig, G. Comelli, A. Baraldi, M. Kiskinova, and R. Rosei, *Phys. Rev. B* **60**, 7800 (1999).
- [49] R. L. Martin and P. J. Hay, *Surf. Sci.* **130**, L283 (1983).
- [50] H. Nakatsuji and H. Nakai, *J. Chem. Phys.* **98**, 2423 (1993).
- [51] J. M. Ricart, J. Torras, A. Clotet, and J. E. Sueiras, *Surf. Sci.* **301**, 89 (1994).
- [52] M. R. Peng and J. E. Reutt-Robey, *Surf. Sci.* **336**, L755 (1995).
- [53] L. Yang and T. S. Rahman, *Surf. Sci.* **215**, 147 (1989).
- [54] S. Narasimhan, *Surf. Sci.* **496**, 331 (2002).
- [55] R. Tatarek, G. Bracco, F. Tommasini, A. Franchini, V. Bortolani, G. Santoro, and R. F. Wallis, *Surf. Sci.* **211**, 314 (1989).
- [56] G. Bracco, L. Bruschi, L. Pedemonte, and R. Tatarek, *Surf. Sci.* **377-379**, 325 (1997).
- [57] S. Lehwald, B. Voigtländer, and H. Ibach, *Phys. Rev. B* **36**, 2446 (1987).
- [58] S. Y. Liem, J. H. R. Clarke, and G. Kresse, *Surf. Sci.* **459**, 104 (2000).
- [59] E. A. Colbourn and J. E. Inglesfield, *Phys. Rev. Lett.* **66**, 2006 (1991).
- [60] L. Vattuone, U. Valbusa, and M. Rocca, *Surf. Sci.* **317**, L1120 (1994).
- [61] C. Åkerlund, I. Zorić, B. Kasemo, A. Cupolillo, F. B. de Mongeot, and M. Rocca, *Chem. Phys. Lett.* **270**, 157 (1997).
- [62] S. Roy, V. Mujica, and M. A. Ratner, *J. Chem. Phys.* **139**, 074702 (2013).
- [63] D. M. Bird and P. A. Gravil, *Surf. Sci.* **377-379**, 555 (1997).
- [64] G. Kresse and D. Joubert, *Phys. Rev. B* **59**, 1758 (1999).
- [65] D. R. Hamann, M. Schlüter, and C. Chiang, *Phys. Rev. Lett.* **43**, 1494 (1979).
- [66] N. Troullier and J. L. Martins, *Phys. Rev. B* **43**, 1993 (1991).
- [67] J. P. Perdew and Y. Wang, *Phys. Rev. B* **45**, 13244 (1992).